JOM, Vol. 69, No. 8, 2017
DOI: 10.1007/s11837-017-2375-x

Novel Electrochemical Test Bench for Evaluating the Functional Fatigue Life of Biomedical Alloys

M.F. IJAZ,[1,3] S. DUBINSKIY,[1] Y. ZHUKOVA,[1] A. KOROBKOVA,[1] Y. PUSTOV,[1] V. BRAILOVSKI,[2] and S. PROKOSHKIN[1,4]

1.—National University of Science and Technology "MISIS", 4 Leninskiy prosp., Moscow, Russian Federation 119049. 2.—Ecole de Technologie Superieure, 1100, rue Notre Dame Ouest, Montreal H3C 1K3, Canada. 3.—e-mail: farzik98@gmail.com. 4.—e-mail: prokoshkin@tmo.misis.ru

The aim of the present work was first to develop and validate a test bench that simulates the in vitro conditions to which the biomedical implants will be actually subjected in vivo. For the preliminary application assessments, the strain-controlled fatigue tests of biomedically pure Ti and Ti–Nb–Zr alloy in simulated body fluid were undertaken. The in situ open-circuit potential measurements from the test bench demonstrated a strong dependence on the dynamic cycling and kind of material under testing. The results showed that during fatigue cycling, the passive oxide film formed on the surface of Ti–Nb–Zr alloy was more resistant to fatigue degradation when compared with pure Ti. The Ti–Nb–Zr alloy exhibited prolonged fatigue life when compared with pure Ti. The fractographic features of both materials were also characterized using scanning electron microscopy. The electrochemical results and the fractographic evidence confirmed that the prolonged functional fatigue life of the Ti–Nb–Zr alloy is apparently ascribable to the reversible martensitic phase transformation.

INTRODUCTION

Among the metallic biomedical materials, the pure Ti, Ti–6Al–4V, and Ti–Ni alloys have been investigated extensively for their diverse applications in the orthopedic and dental fields. Nevertheless, for the long-term survival of indwelling implants, the hypersensitivity of nickel and toxicity of vanadium has become an issue of widespread concern.[1] On the other hand, although pure Ti (also known as CP Ti) has excellent biocompatibility, its applications are limited because of its poor mechanical properties.[1,2] Therefore, to circumvent these challenging problems, rigorous endeavors have been undertaken to explore the new generation of Ni- and V-free biomedical alloys.[2–6] In this context, superelastic beta titanium alloys seems conducive to future implant applications.[2–11]

Nevertheless, during service, the implants are commonly subjected to cyclic fatigue under the corrosive physiological conditions of the human body.[2,5,12] In fact, the destructive nature of the corrosion-assisted fatigue cracking and overall fatigue degradation can incapacitate the long-term performance of implants.[12–15] Therefore, it is vital to investigate the functional fatigue life under physiological conditions. Despite all its practical relevance, the specific pseudo-physiological test bench for evaluating the functional fatigue life of the superelastic beta titanium alloys and corresponding in situ electrochemical results revealing the impact of cycling on the corrosive and passive behavior for this kind of alloys are sparse in the literature and hence require more research.

Our current strategy is motivated by our previous works, which were done to investigate the corrosion fatigue properties under the applied strain value only limited to 0.8%.[11,13,16] Nonetheless, from the viewpoint of practical applications, it is essential to monitor the functional fatigue performance of new biomedical alloys at higher strain amplitude conditions.[11]

In this context, one objective of this work is to design a novel multifunctional physiological test bench for evaluating the functional fatigue characteristics under dynamic mechanical cycling. Subsequently, the preliminary experimental results on the corrosive and passive behavior of recently

(Published online May 18, 2017)

developed Ti–22Nb–6Zr alloy[3,5,11] were investigated and discussed in comparison with the commercially available implant materials, i.e., pure Ti (Grade-2).[1,2]

EXPERIMENTAL

Alloy Synthesis and Specimen Preparation

The Ti–22Nb–6Zr (at.%) alloy (hereinafter referred to as Ti–Nb–Zr) was synthesized by the vacuum arc-melting method. After the melting procedure, the 80-mm-diameter ingot was hot forged at 1173 K and machined to a 50 mm diameter after quenching. Next, the ingot was subjected to a series of thermomechanical treatments that included multipass hot-rolling, rotational-forging, and cold-drawing operations with intermediate annealing treatments until the accumulated true strain approached $e = 0.3$ in the final passes.[11] The final diameter of the cold drawn wire specimen is 0.5 mm. Subsequently, the cold-drawn wire specimen was subjected to post-deformation annealing (PDA) at 873 K for 1.8 ks followed by quenching in water. Accordingly, the commercially available α-type pure Ti (hereinafter referred as Ti) was also heat treated at 973 K for 1.8 ks mainly to establish the recrystallized state. Eventually, to remove the slightly oxidized surface, all the heat-treated specimens were mechanically abraded by fine silicon carbide abrasive paper.

Alloy Characterization Method

To have an insight into microstructural morphology, transmission electron microscopy (TEM) observations were performed on the disk-shaped Ti–Nb–Zr alloy thin foils with a standard grid size of 3.05 mm. A JEM-2100 (JEOL Ltd./Japan) TEM operating at 200-kV accelerating voltage, with a camera length of 25 cm was used. Specimens for TEM analysis were prepared from the sheet with a consistent thermomechanical treatments.[11]

Electrochemical Behavior Testing

During the fatigue test, the electrochemical investigations were based on conventional open-circuit potential (OCP) measurements that were performed using IPC Pro MF potentiostat (Volta Co, Russia) at 298 K. The electrolyte used for the electrochemical analysis was 0.9% NaCl physiological solution (Braun, Germany).

Fractography of the Specimen After Fatigue Testing

The fracture surfaces after the dynamic fatigue fracture were investigated using a Vegas-Tescan scanning electron microscope (SEM) at an accelerating voltage of 20 kV and a working distance of 15 mm.

Design and Manufacturing of Test Bench for the Electrochemical Examinations During Fatigue Test

The schematic and simplified representation of the self-designed experimental setup used for the in situ electrochemical testing of the specimen that is cyclically deformed and at the same time exposed constantly to the corrosive environment is shown in Fig. 1. Our indigenously manufactured pseudo-physiological test bench mainly consists of a thermally controlled sealed basin, an electrolyte apparatus, electrically isolated specimen chucks, wire-shaped specimen acting as the working electrode (WE), potentiostat, moveable machine crosshead, servo cell, programmable microcontroller, and Arduino data acquisition system. The wire-shaped test specimen with the gauge length of 10 cm (as indicated in Fig. 1) is affixed between the rotating chucks. The chucks represented in Fig. 1 are attached to the precision displacement stage (machine crosshead) that induces periodic cycling. In fact, while carrying out the strain-controlled dynamic fatigue tests in a physiological solution, the test specimen was subjected to cycling loading–unloading by using a servo-motor and system. An optimum loading frequency of 0.9 Hz and a constant dynamic strain of 1.5% were used in each cycle until fracture. Here, a large imposed strain value of 1.5% was selected because it roughly corresponds to the distinct superelastic domain of the currently investigated Ti–Nb–Zr alloy.[5,11] The electrochemical potentials were simultaneously measured against a reference saturated silver chloride electrode (Ag/AgCl) (RE). Two separate and respective OCP responses were also recorded at each steady and dynamic-cycling state.

RESULTS AND DISCUSSION

Microstructure of the Ti–Nb–Zr Alloy

Figure 2a and b shows the respective bright and dark field images and corresponding selected diffraction pattern with zone axis $[1\bar{2}0]_\beta$ of the Ti–Nb–Zr alloy after thermomechanical treatments. The selected area diffraction pattern reveals only β-phase reflections. The dark field image is obtained while using the $(\bar{2}\bar{1}\bar{1})$ reflection of the β-phase (as encircled in Fig. 2b). The microstructure mainly consists of grain-like constituents with a diameter ranging from 50 to 200 nm as shown in Fig. 2a. These unique microstructural features are in fact the subgrains engendered as a result of the polygonization process during PDA at 873 K.[5,11] This subgrain structure can also be indirectly evident from the low-angle azimuthal broadening of the β-phase spots as revealed in the corresponding selected area diffraction pattern (Fig. 2b).

Electrochemical and Corrosion Behavior of Studied Materials During Cyclic Fatigue Test

Figure 3a displays the OCP values (mV) as a function of exposure time (s) for the Ti and Ti–Nb–Zr alloy specimens subjected to cyclic fatigue test in 0.9% NaCl physiological solution. The summary of the experimental results is also listed in Table I. For better understanding, the OCP response of Ti and Ti–Nb–Zr alloy specimens particularly at the steady state (E_{st}) and at the start of the cycling states (E_c) are truncated from the entire OCP plots and shown separately in Fig. 3b. The respective ΔE, which is the difference between the E_{st} and the E_c for the Ti and Ti–Nb–Zr alloy specimens is also distinguished by the dotted line and is shown in Fig. 3b.

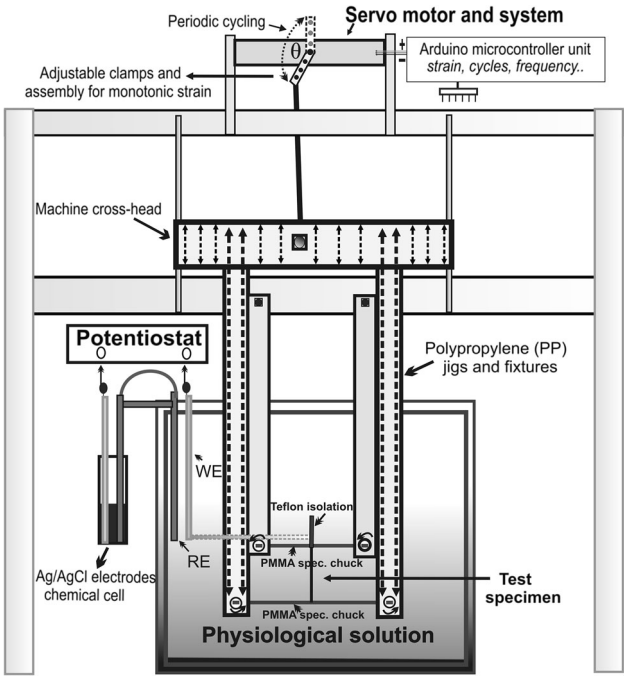

Fig. 1. Schematic illustration of the experimental test bench used for monitoring the influence of cyclic fatigue on the electrochemical behavior of biomedical alloys in physiological solution.

Fatigue cycling was imposed after the establishment of their respective time-invariant steady states. The E_{st} value of Ti–Nb–Zr alloy (–56 mV) is slightly higher than that of Ti (–87 mV). Once the respective E_{st} for both specimens was achieved, the repeated cycling with a constant strain amplitude of 1.5% was imposed. It can be observed that after the initiation of dynamic cycling, the OCP for both Ti and Ti–Nb–Zr alloy specimens shifted toward the negative values. Nonetheless, these shifts in the OCP toward negative potentials are attributed to the abrupt cathodic polarizations. Nevertheless, in the case of Ti specimen, the potential change in the negative direction is sharp. Indeed the E_c values for the Ti and Ti–Nb–Zr alloy specimens are about −413 and −199 mV, respectively.

Apart from that, the ΔE is larger for the Ti specimens when compared with the Ti–Nb–Zr alloy specimen (as shown in Fig. 3b). It implies that the passive oxide film is more stable upon cycling in the case of the Ti–Nb–Zr alloy specimen. Meanwhile, it can also be observed that during the initial period of cycling, the E_c of Ti shifts toward the positive direction with time at the first 50 s, which may be ascribable to the recovery of the mechanically destroyed film, as well as by plastifying impact of the chemomechanical effect.[16] However, later the E_c of Ti monotonically shifts toward the negative direction until fracture, essentially resulting from the local rupture of the protective film or from the dissolution of the film prevailing over its formation.[12–18]

On the other hand, the E_c of the Ti–Nb–Zr alloy specimen exhibits an increasing tendency with the time duration for about 400 s and then maintains a relatively stable value. Consequently, the protective passive films begin to grow on the Ti–Nb–Zr alloy specimen surface and then forms a stable passive film during the cycling. Another reason for this

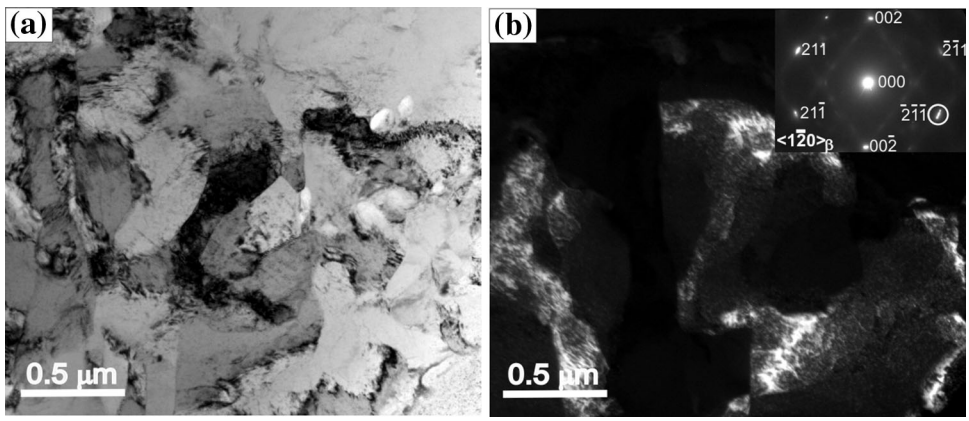

Fig. 2. Transmission electron microscopy (a) bright field image and (b) dark field image with a selected area diffraction pattern (shown in inset) of Ti–Nb–Zr alloy specimen after PDA at 873 K for 1.8 ks.

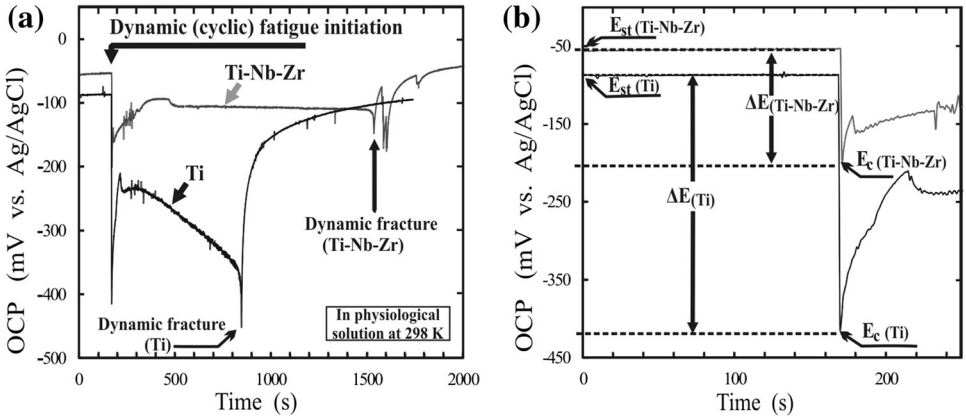

Fig. 3. (a) Comparison of the OCP curves acquired during the cyclic fatigue testing of the Ti and Ti–Nb–Zr alloy specimens while imposing a constant strain amplitude of 1.5% and (b) OCP curves zoomed around the evolution of the steady (E_{st}) and cyclic (E_c) response under dynamic (cyclic) fatigue testing of the Ti and Ti–Nb–Zr alloy specimens.

Table I. Comparison of the experimental results from fatigue testing of the selected biomedical materials in the pseudo-physiological test bench

		***E* (mV) (Ag/AgCl)**		
Materials	**Number of fatigue cycles to dynamic fracture (N_f)**	E_{st}	E_c	$\Delta E_{(E_{st}-E_c)}$
Pure Ti	750	−87	−413	−326
Ti–Nb–Zr alloy	1516	−56	−199	−143

stable passive film may be because of the "mechanochemical effect," which is elicited at the specimen–electrolyte interface.[13,16]

Nevertheless, when the dynamic fracture stage for both specimens was approached (as pointed in Fig. 3a), a slight but distinct negative shift in the OCP values corresponding to fracture was observed that was followed by a rapid shift in the positive direction implying the passivation of the freshly formed surface.[12,13,16] From OCP plots, the dynamic fracture stage for the Ti and Ti–Nb–Zr alloy specimens are precisely estimated to occur around the exposure time of 846 s (E_c = –451 mV) for Ti and 1536 s (E_c = –147 mV) for Ti–Nb–Zr alloy, respectively. Based on these results, it can be concluded that the Ti–Nb–Zr alloy possesses a better corrosion resistance under dynamic cycling as a result of the higher stability of protective oxide film that is also evident from the steady OCP variations of Ti–Nb–Zr alloy when compared with Ti.

Finally, while comparing the corresponding fatigue life (a total number of fatigue cycles N_f) of Ti and Ti–Nb–Zr alloy specimens, the N_f values for Ti and Ti–Nb–Zr alloy specimens in the physiological solution are calculated to be 750 and 1516 cycles, respectively.

Fractographic Analysis of the Dynamically Fractured Specimens

To discuss the pronounced fatigue lifetime of Ti–Nb–Zr alloy in the physiological solution, the apparent surface components of the fracture surfaces of Ti and Ti–Nb–Zr alloy specimens were systematically compared. Figure 4a–d shows the general fractography of Ti and Ti–Nb–Zr alloy specimens, which were characterized by SEM. The sequential elaboration of the macroscopic and microscopic regions for Ti and Ti–Nb–Zr alloy specimens, particularly the crack origin, fatigue crack propagation region, and final unstable region that is near the edge, is also illustrated in Fig. 4a and c, respectively. On the other hand, for the sake of clarity, an example showing the segment of fatigue striations by the crack propagation in the stable region and dimples at the unstable region are also highlighted with the white rectangular boxes and shown in Fig. 4b and d, respectively. From general aspects, it is evident that the dynamic fracture in both specimens was elicited mainly by a transgranular pattern[12,14–16] as the corresponding three regions (as shown in Fig. 4a–d) are easily identifiable.

In particular, from Fig. 4a and b, it is also noteworthy that in the case of the Ti specimen, the stable region showing the fatigue crack propagation is much smaller than the final overloaded region. In fact, the enlarged unstable zone of Ti (as shown in Fig. 4a and b) on the one hand corroborates the pronounced shift of the E_c value toward the negative potentials (as shown in Fig. 3a and b). Nonetheless, during the fatigue testing of the Ti specimen, the subsequent rapture of the local passive film caused by the influence of cycling has

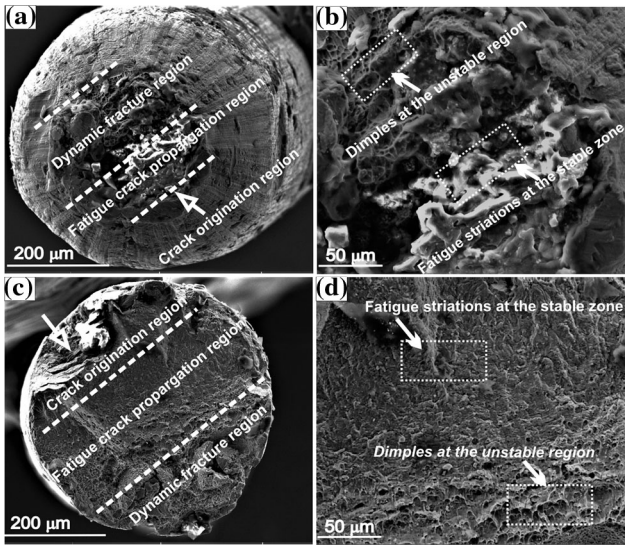

Fig. 4. SEM micrographs show the comparison of the overall fracture surfaces of (a, b) Ti and (c, d) Ti–Nb–Zr alloy specimens after cyclic fatigue testing in physiological solution.

accelerated the corrosion-assisted fatigue crack growth in the localized unstable zone, which has ultimately led to the dynamic fatigue fracture and relatively shorter fatigue life.

Surprisingly, the fractography of the Ti–Nb–Zr alloy specimen (as shown in Fig. 4c and d) clearly demonstrates a much larger fatigue striation region when compared with the Ti specimen (as shown in Fig. 4a and b). It is previously reported that in a physiological solution, the stress-induced martensitic transformation during loading/unloading cycles can prevent the spreading of the crack and enhance the plastic properties of surface layers.[13,16]

Finally, by correlating the microstructural results with the OCP response, it is summarized that the increase in the fatigue life of Ti–Nb–Zr alloy is first related to the stable passive film formation that inhibits the local corrosive attack and second to the reversible stress-induced martensitic transformation[5,13,14,16] that can accommodate the material strains during subsequent unloading cycle and eventually preclude the dynamic fatigue fracture for a longer period of time.

CONCLUSION

In conclusion, for the successful applications of the recently developed biomedical alloys in the potential indwelling implant applications, it is important to evaluate their functional fatigue performance in physiological conditions. In this context, a novel pseudo-physiological test bench was specifically designed and manufactured. Next, the test bench was validated while using recently developed superelastic Ti–Nb–Zr alloy and pure Ti. Experimental results have revealed that under dynamic cycling, the Ti–Nb–Zr alloy specimen exhibits higher cyclic state open-circuit potential values (E_c) and its passive oxide film is more stable when compared with pure Ti specimen. The Ti–Nb–Zr alloy manifests a much longer functional fatigue life as well. Fractographical characteristics after fatigue fracture showed that the comparatively longer fatigue life of Ti–Nb–Zr alloy could be correlated with the appearance of a large fatigue striations region that has engendered from the reversible stress-induced martensitic transformation. Based on these conclusions, which have been reproduced from our test bench, it is suggested that for advanced biomedical applications, the Ti–Nb–Zr alloy is less susceptible to fatigue degradation when compared with pure Ti.

ACKNOWLEDGEMENTS

The authors acknowledge Dr. Andrey Korotitskiy for his valuable participation in the test bench design. The present work was carried out with the financial support of the Ministry of Education and Science of the Russian Federation, in the framework of the Increase Competitiveness Program of NUST "MISIS" (Grant К4-2016-56), and of the Natural Science and Engineering Research Council of Canada (NSERC), the Fonds de Recherche Nature et Technology du Quèbec (FQR-NT).

REFERENCES

1. C.N. Elias, J.H.C. Lima, R. Valiev, and M.A. Meyers, *JOM* 60, 46 (2008).
2. M. Niinomi, Y. Liu, M. Nakai, and H. Liu, *Regen. Biomater.* 3, 173 (2016).
3. T. Yoneyama and S. Miyazaki, *Shape Memory Alloys for Biomedical Applications* (Cambridge: Woodhead Publishing, 2009).
4. H.Y. Kim and S. Miyazaki, *Shape Mem. Superelasticity* 2, 380 (2016).
5. S. Prokoshkin, V. Brailovski, S. Dubinsky, Y. Zhukova, V. Sheremetyev, A. Konopatsky, and K. Inaekyan, *Shape Mem. Superelasticity* 2, 130 (2016).
6. P. Castany, A. Ramarolahy, F. Prima, P. Laheurte, C. Curfs, and T. Gloriant, *Acta Mater.* 88, 102 (2015).
7. M.F. Ijaz, H.Y. Kim, H. Hosoda, and S. Miyazaki, *Scripta Mater.* 72–73, 29 (2014).
8. P. Xue, Y. Li, F. Zhang, and C. Zhou, *Scripta Mater.* 101, 99 (2015).
9. M.F. Ijaz, H.Y. Kim, H. Hosoda, and S. Miyazaki, *Mater. Sci. Eng., C* 48, 11 (2015).
10. M.F. Ijaz, D. Laille, L. Heraud, D.M. Gordin, P. Castany, and T. Gloriant, *Mater. Lett.* 177, 39 (2016).
11. S.M. Dubinskiy, S.D. Prokoshkin, V. Brailovski, K.E. Inaekyan, A.V. Korotitskiy, M.R. Filonov, and M.I. Petrzhik, *Phys. Met. Metallogr.* 112, 503 (2011).
12. ASTM F 1801–1997, *Standard Practice for Corrosion Fatigue Testing of Metallic Implant Material* (2004).
13. Y.S. Zhukova, Y.A. Pustov, A.S. Konopatsky, S.M. Dubinskiy, M.R. Filonov, and V. Brailovski, *Mater. Today Proc.* 2S, S991 (2015).
14. Y.L. Zhou, M. Niinomi, and T. Akahori, *Mater. Trans.* 45, 1549 (2004).
15. L.C. Campanelli, C.C. Bortlan, P.S. Carvalho da Silva, C. Bolfarini, and N.T.C. Oliveira, *J. Mech. Behav. Biomed.* 65, 542 (2017).

16. Y.A. Pustov, Y.S. Zhukova, and M.R. Filonov, *Prot. Met. Phys. Chem. Surf.* 50, 524 (2014).
17. L. Qiang, L. Junjie, M. Guanghao, L. Xuyan, and P. Deng, *Mater. Des.* 111, 421 (2016).
18. R. Ion, S.I. Drob, M.F. Ijaz, C. Vasilescu, P. Osiceanu, D.M. Gordin, A. Cimpean, and T. Gloriant, *Materials* 9, 818 (2016).